Int. J. Multiphase Flow Vol. 16, No. 6, pp. 1097–1116, 1990
Printed in Great Britain

0301-9322/90 $3.00 + 0.00
Pergamon Press/Elsevier

TIME-DEPENDENT BEHAVIOUR OF THE LIQUID FILM IN HORIZONTAL ANNULAR FLOW

S. JAYANTI,[1] G. F. HEWITT[1,2] and S. P. WHITE[1]

[1]Department of Chemical Engineering and Chemical Technology, Imperial College of Science, Technology and Medicine, London SW7 2BY, England

[2]Thermal Hydraulics Division, Harwell Laboratory, Didcot, Oxon. OX11 0RA, England

(*Received* 28 *August* 1989; *in revised form* 18 *June* 1990)

Abstract—A crucial point still to be established in the prediction of the film thickness distribution in horizontal annular two-phase flow is the mechanism(s) for transporting liquid from the bottom to the top part of the tube. To resolve this issue, the time-dependent behaviour of the liquid film is studied. Wave characteristics such as velocity and frequency are measured around the circumference. It is inferred from the autospectral density functions of film thickness variation that disturbance waves play an important, but as yet unclear, role in the formation of a liquid film in the top part of the tube. A new mechanism, based on the shape of disturbance waves is proposed.

Key Words: horizontal annular flow, film thickness variation, conductance probes, spectral analysis, disturbance waves, wave characteristics, wave spreading mechanism

1. INTRODUCTION

An important feature of horizontal annular flow is the effect of gravity, because of which the liquid in the upper part of the tube tends to drain down the wall towards the bottom. Thus, for annular flow to occur, there must be a means of transporting liquid from the bottom to the top to counter this drainage. These mechanisms must be identified and modelled in order to develop an accurate predictive model for horizontal annular flow. Several such mechanisms have been proposed over the years; the more important and credible among these are:

(a) Secondary flow mechanism [first proposed by Pletcher & McManus (1965), and recently modelled quantitatively by Laurinat *et al.* (1985) and Lin *et al.* (1985)], where the circumferential variation of the film thickness subjects the gas phase to a circumferentially varying interfacial roughness. This creates a two-vortex secondary flow in the gas phase, which drives the liquid up along the wall.
(b) Entrainment and redeposition mechanism [proposed by Russell (1965), and studied later by Anderson (1968) and Wilkes *et al.* (1980) etc.], where a net entrainment flux from the bottom to the top of the tube is created by the variation in the film thickness.
(c) Wave spreading mechanism (Butterworth 1971), where the wave front gets distorted as the wave crest moves faster at the bottom of the tube. This induces a circumferential component of the force exerted by the gas phase on the wave which drives liquid up the wall.
(d) Pumping action due to a disturbance wave (Fukano & Ousaka 1989), where the gas flow over a disturbance wave is assumed to create a circumferential pressure gradient due to the variation in the wave amplitude. Oliemans & Ooms (1986) associated a similar circumferential pressure gradient with ripple waves in oil–water core annular flow, where the oil core is laminar.

Several experiments have been carried out to verify the existence of these mechanisms in horizontal annular flow. Anderson (1968), Butterworth & Pulling (1972) and Hewitt *et al.* (1989) conducted dye tracing experiments to visualize the flow in the liquid phase. Anderson (1968) found that the liquid film was periodically moving upwards and draining down, indicating possible wave action. Such oscillation did not occur if most of the liquid film was removed through a porous

sinter. Butterworth & Pulling (1972) and Hewitt *et al.* (1989) found that the dispersion of the dye in a disturbance wave was too quick to detect any secondary flow in the wave. In support of the secondary flow mechanism, Darling & McManus (1968) demonstrated that a two-vortex secondary flow would be created in single-phase flow through a differentially roughened tube. However, such flow, or its effect on the motion of liquid droplets, has not been observed in annular two-phase flow.

There have been several quantitative estimates of the contribution of the various mechanisms to the liquid film distribution in horizontal annular flow. Wilkes *et al.* (1980) modelled the effect of gravity on droplet motion, and demonstrated that the film thickness data of Butterworth (1971) and Pearce & Fisher (1976) could be predicted fairly well by the entrainment–redeposition mechanism. However, this mechanism was found to be of negligible importance by Laurinat *et al.* (1985), Lin *et al.* (1985) and Fukano & Ousaka (1989), none of whom consider the effect of gravity on droplet deposition. There was a similar discrepancy between the results of Fukano & Ousaka (1989) and Laurinat *et al.* (1985) and Lin *et al.* (1985). For similar flow conditions, each group was able to predict the film thickness distribution using different transport mechanisms. Thus, there is a general lack of consensus among these numerical models as to the dominant mechanism(s) of horizontal annular flow. The reason lies mainly in the inadequate modelling and characterization—prompted perhaps by a paucity of experimental data—of the mechanisms themselves.

Against this background, the purpose of the work presented here is two-fold: (1) to study the time-dependent behaviour of the liquid film in order to obtain the dynamic characteristics necessary to understand and model the interface phenomena; and (2) to investigate the validity of the various mechanisms in light of these experimental results. To this end, we use statistical/spectral techniques to analyse the film thickness measured by conductance probes. Such techniques have been used previously by Webb (1970) and Martin & Azzopardi (1985) for vertical annular flow. Pearce (1979) and Fukano *et al.* (1983) used them in horizontal annular flow but their experiments were not designed to test the presence or otherwise of the mechanisms themselves.

2. EXPERIMENTAL WORK

2.1. Film thickness measurements

Film thickness measurements were carried out in the air–water horizontal flow rig shown schematically in figure 1. The test section is a 5.5 m long acrylic resin tube of 32 mm i.d. Air enters the test section at one end from a compressed air supply. Water is injected through a porous tube wall section. The film thickness was measured at a distance of 3.5 m from the porous wall injector, thus giving a developing length of 110 tube diameters. In view of the fact that water entered through a porous wall section, it was felt that this length was sufficient for the flow to be fully developed. Recent measurements at 175 tube diameters confirm this.

The air flow rate to the test section was measured by an orifice plate. Rotameters were used to measure the water flow rate. Pin-type conductance probes were used to measure the film thickness at two positions simultaneously. The probes were set in acrylic resin blocks bored out to the same inner diameter as the test section tube. The conducting material was made of a stainless steel rod and was glued into the resin block. The voltage drop across the probes was measured using a digital multimeter. The potential difference across the probes was produced by a signal generator operating at 21 kHz. This made conductivity changes due to electrolysis negligible. The output from the probes was also displayed on an oscilloscope. An EMI 3000 tape recorder was used to record the analogue outputs from the two probes. The probe geometry and the circuit diagram for the measurement system are shown in figures 2(a,b). The conductance probes were calibrated using epoxy resin plugs which were machined such that a known film thickness could be maintained between the plug and the probe surface. A special fixture with a dial gauge mounted on it was used to reduce the error in locating the plug correctly. The calibration was carried out using eight plugs giving a film thickness range of 0.2–3 mm.

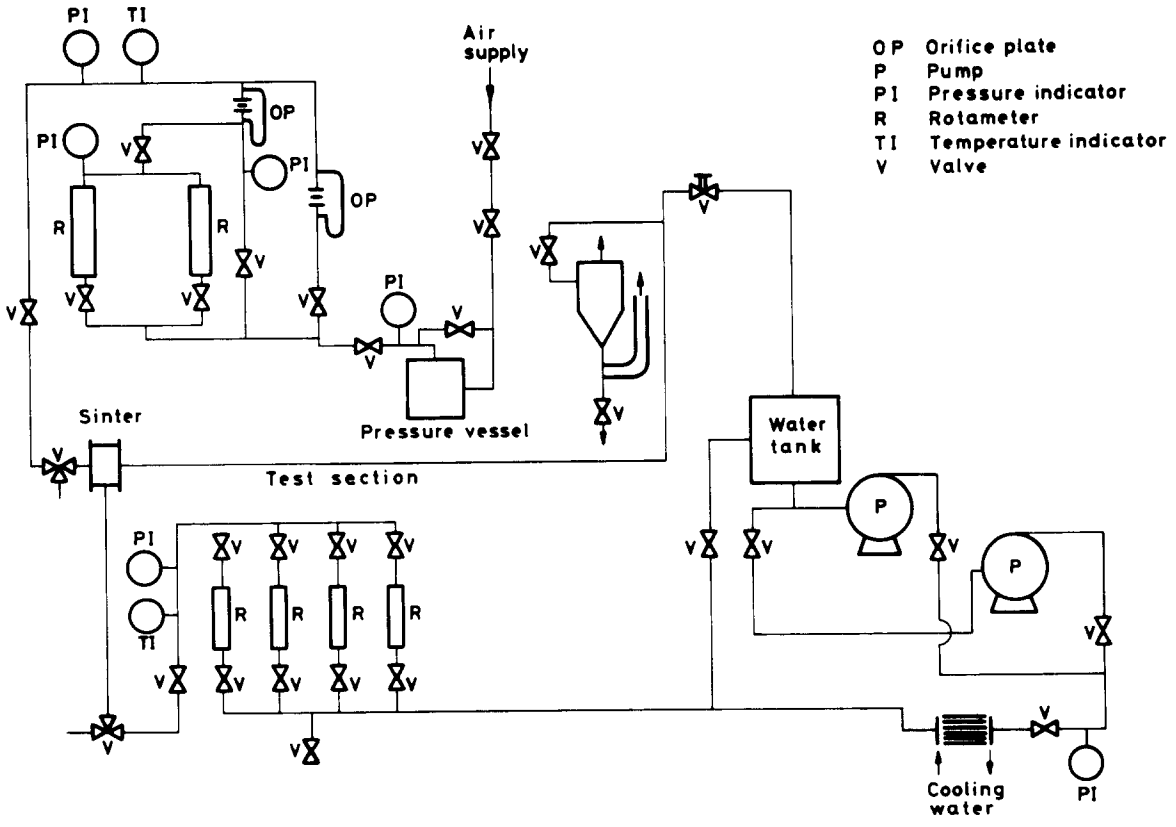

Figure 1. Schematic diagram of the experimental rig.

Film thickness was measured for five different combinations of air and water flow rates, as shown in table 1. Visual observations as well as film thickness signals showed that the flow pattern was annular in all cases. Film thickness was measured at five circumferential positions—0° (bottom), 45°, 90°, 135° and 180°. For each run, four probes, say, A, B, C and D were located such that probes A & C were at one circumferential position, say, at 45° from the bottom, and probes B & D were at, say, 135° (see figure 3). Both probes A & C and B & D were separated by an axial distance of 0.133 m. A relay switch was used to select any two of the four probes for recording simultaneously. In a typical run, the film thickness at A & C, that at B & D, and that at A & D were recorded simultaneously. This made it possible to correlate the film thickness both axially and circumferentially. Each recording lasted 3 min. The temperature of the air or of the circulating water varied typically between 19–21°C for air and between 18–20°C for water. The overall pressure in the test section varied with flow rates due to the creation of back pressure from the test section outlet. However, the pressure at the probe assembly was noted, and was used to calculate the fluid properties in the results given below.

2.2. Data analysis

A typical output signal from the conductance probe is shown in figure 4. It can be seen that the signal fluctuates rapidly and it is best processed by statistical methods. To this end, two systems were used: an analogue Solartron 1200 Signal Processor; and a digital software package called Data Analysis Terminal Systems (DATS) from Prosig Consultants Co. (It is heartening to note that both systems gave similar results!) Apart from the conversion of the voltage signal to the film thickness signal using DATS, the following statistical functions were calculated using both systems: autospectral density (ASD) function: cross-spectral density (CSD) function; cross-correlation function (CCF) in the time domain; and coherence function. For the definition and physical interpretation of these functions the reader is referred to the excellent book by Bendat & Pearson (1986). The results are discussed below.

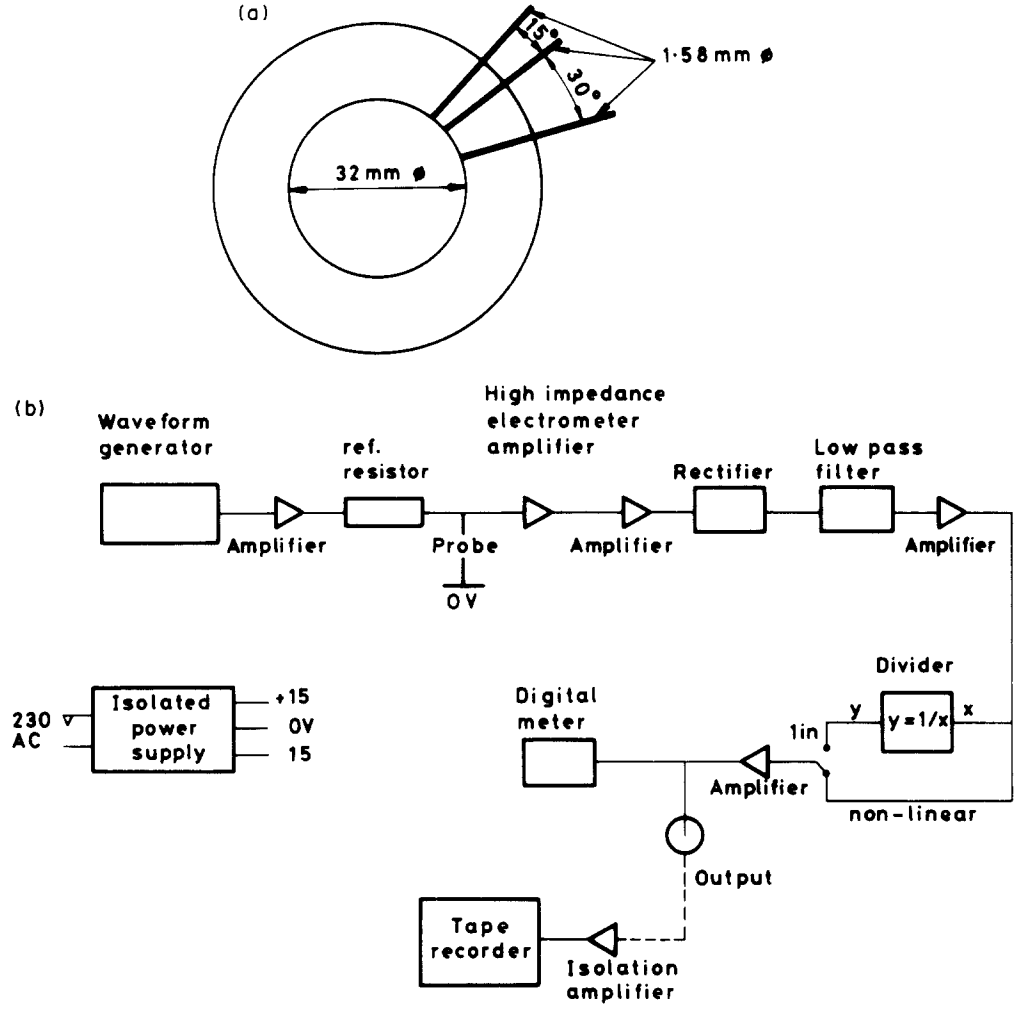

Figure 2. (a) Probe geometry and (b) circuit diagram.

3. RESULTS AND DISCUSSION

3.1. *Variation of film thickness with time*

Figures 5(a–c) show the variation of the film thickness with time for a water flow rate of 0.064 kg/s and an air flow rate of 0.026 kg/s at 0° (bottom part of the tube), 90° and 180° (top). Note that the scales on the axes are different. It can be seen that the film at the bottom part is very agitated and is characterized by rather regular "disturbance" waves with an amplitude of up to 3–4 mm. At 90° the film shows similar variation with time, although the maximum height is only of the order 0.5 mm. At the top, the film shows a markedly different behaviour: it is wetted

Table 1. Experimental conditions

S. No.	Water flow rate ($kg\,s^{-1}$)	Air flow rate ($kg\,s^{-1}$)	Test section pressure (bar)	Air density ($kg\,m^{-3}$)	Superficial velocity		Re[a]	
					Air ($m\,s^{-1}$)	Water ($m\,s^{-1}$)	Air	Water
1	0.118	0.026	1.75	2.26	14.3	0.145	57500	4640
2	0.098	0.026	1.68	2.18	14.9	0.119	57500	3800
3	0.064	0.026	1.61	2.08	15.5	0.080	57500	2560
4	0.064	0.053	2.16	2.79	23.6	0.080	117000	2560
5	0.064	0.065	2.43	3.14	25.7	0.080	117000	2560

Working fluids: air and water. Tube i.d. = 0.032 m; developing length = 3.6 m; test section pressure = 1.5 to 2.5 bar; density of water = 1000 $kg\,m^{-3}$; viscosity of water = 1.0×10^{-3} $N\,s\,m^{-2}$; viscosity of air = 1.8×10^{-5} $N\,s\,m^{-2}$.
[a]Based on the tube diameter and the superficial gas velocity.

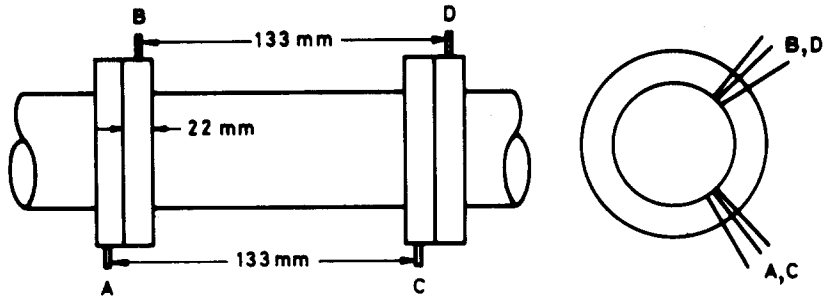

Figure 3. Typical arrangement of probes.

periodically by waves (or surges) of much lower frequency (of the order of 1 Hz), with the film draining down between these surges. At the higher gas phase velocities, such surges may not occur.

Figures 6(a–c) show the ASD functions of the film thickness for the cases shown in figures 5(a–c). The occurrence of a maximum in an ASD may indicate the presence of a periodic phenomenon such as the disturbance waves. In figures 6(a–c), all the ASD functions show a maximum, although at different frequencies. The dominant frequency at the bottom part of the tube, corresponding to the disturbance wave frequency, is about 5 Hz. Thus, it can be said that for this set of flow conditions, the disturbance waves are not circumferentially coherent, and that the liquid film at the top is affected mainly by low frequency waves.

Figures 7(a–c) show the variation of film thickness at a higher liquid flow rate but at the same circumferential positions. Now the height of the disturbance waves increases to at least 5 mm, and the conductance probes are probably saturated. As will be shown below, these waves propagate with a speed of the order of 2 m/s, thus their wavelength is of the order of 0.25 m. The liquid film at the side shows the same temporal variation as at the bottom, while the top of the tube is still wetted by low frequency surges. These results are consistent with those of Coney (1971) and Krasiakova (1952), who observed that for low gas flow rates, the film at the top is wetted mainly by frothy surges of liquid. Figures 8(a–c) show the ASD functions corresponding to these cases. It can be seen that the disturbance wave frequency has decreased slightly to about 3–4 Hz, whereas the surge frequency has increased. This is contrary to what happens in vertical annular flow; wherein the disturbance wave frequency increases slightly as the liquid flow rate is increased (Martin & Azzopardi 1985).

Figures 9(a–c) and 10(a–c) show the variation of film thickness at a much higher gas flow rate. It can be seen in figures 9(a–c) that the film is much thinner at the bottom part, with the disturbance waves having an amplitude of about 1–2 mm. Also, they occur intermittently, whereas the waves in figures 5(a–c) and 7(a–c) are almost continuous. The corresponding ASD in figures 10(a–c) show that range of dominant frequencies is much wider, between 5 and 20 Hz. The liquid film at the side and the top of the tube also shows similar behaviour, thus showing perhaps that the disturbance

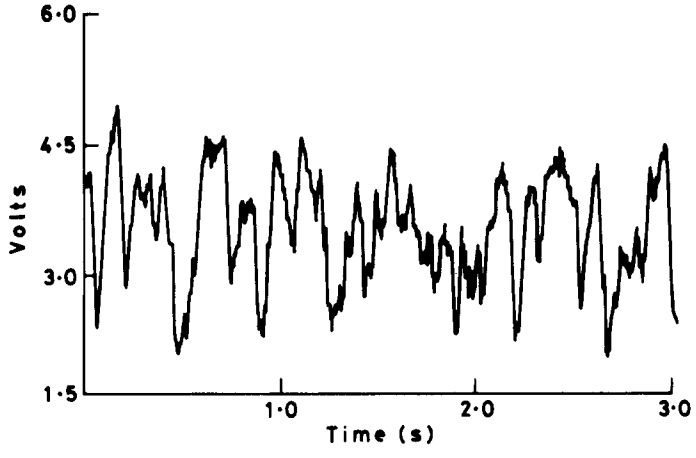

Figure 4. Typical signal from a probe.

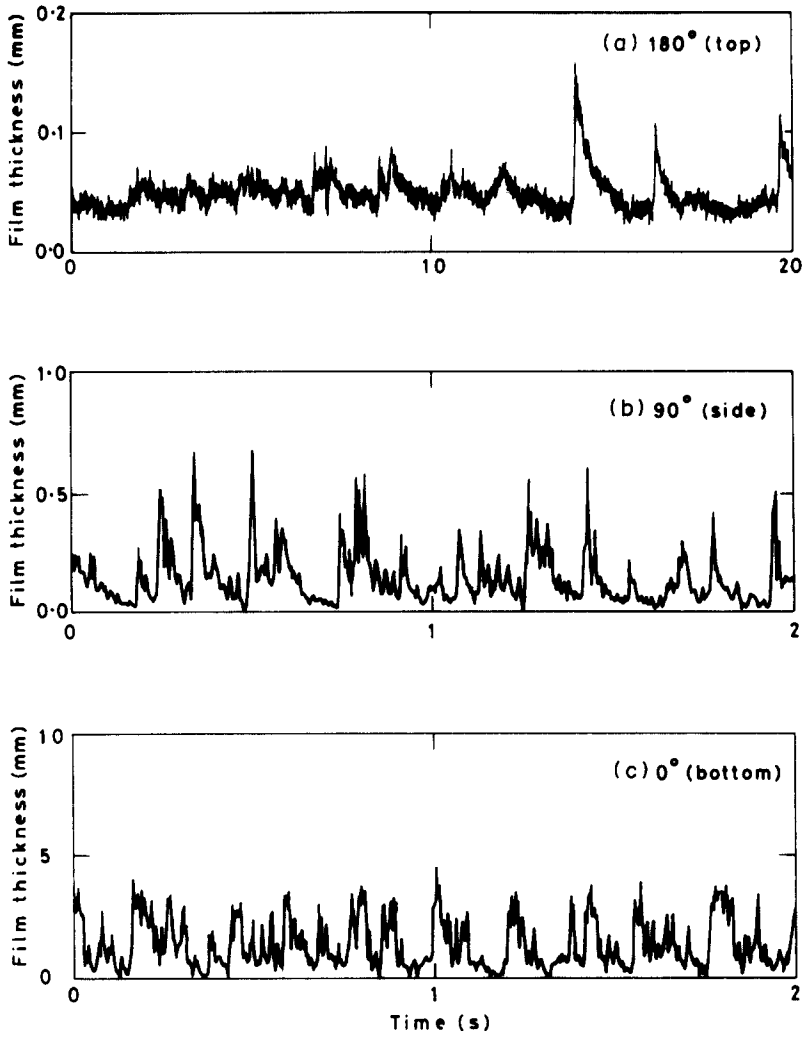

Figure 5. Variation of film thickness with time; liquid flow rate = 0.064 kg/s and gas flow rate = 0.026 kg/s.

waves now spread all around the tube periphery. There is very little contribution, if any, to the film at the top from low frequency surges. At the higher gas phase velocities, such surges may not occur.

Figures 11(a–e) show the nature of the disturbance waves in the bottom part of the tube for decreasing liquid flow rate [figures 11(a–c)] and increasing gas flow rate [figures 11(c–e)]. It can be seen that the wave height increases with liquid flow rate (this effect is obscured to some extent by the saturation of the conductance probes), and decreases with gas flow rate. The ratio of wave height to the mean film thickness is about 4–5, although the conductance probes appear to be saturated in figures 11(a, b). The waves are almost continuous at high liquid flow rates with a wavelength of about 0.3–0.4 m, and tend to break up into smaller waves [figure 11(a)]. This can also be seen in the corresponding ASD function [figure 8(a)], where secondary peaks appear at higher frequencies. As the liquid flow rate decreases or the gas flow rate increases, the waves become more intermittent, and more frequent. Thus, the transition from long waves in figure 11(a) to short intermittent peaks in figure 11(e) appears to be a result of successive breaking up due to interaction with the gas phase.

3.2. Mean film thickness

The variation with flow conditions and circumferential position of the mean film thickness, obtained by numerically time-averaging the film thickness signal, is shown in table 2. At low gas flow rates, the film thickness changes little in the upper half of the tube; it decreases drastically

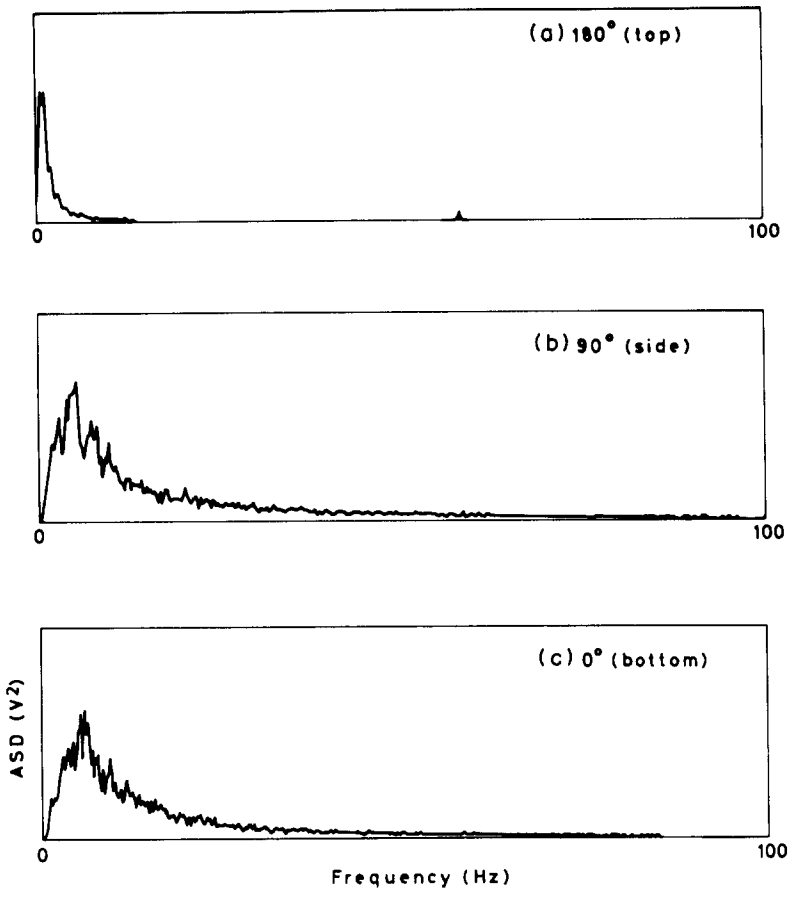

Figure 6. ASDs of the film thickness variation; water flow rate = 0.064 kg/s and air flow rate = 0.026 kg/s.

between 45° and 90°. As the gas flow rate increases, the film tends to become more uniform. However, there is very little variation of film thickness in the upper part of the tube. Thus, the uniformity in the film thickness is due more to the thinning of the film at the bottom than to circumferential redistribution. The same behaviour can be found in the results of McManus (1959) and Butterworth (1971), among others.

3.3. Wave speeds

Wave velocities can be obtained by cross-correlating the film thickness measured simultaneously by two probes separated by an axial distance, Δz. The time at which a peak occurs in the CCF is the time taken for a wave to travel the distance Δz, from which the wave velocity can be calculated (see figure 12). If there are no waves, or if the waves are not coherent over the axial distance Δz, which may happen for ripple waves, there will not be a peak in the CCF. A typical CCF obtained in our experiments is shown in figure 12.

Figure 13 shows the wave velocities thus calculated at various circumferential positions as a function of the flow conditions. It is immediately seen that waves travel faster when the gas flow rate increases, and that the liquid flow rate does not have a significant effect on the wave velocity. A rather surprising result is that the wave velocity is higher in the upper part of the tube than in the lower part. It is tempting to dismiss this as due to experimental error, but the variation of wave velocity is too consistent to be attributed to *random* error. The film thickness was measured under fairly steady-state conditions, and a relay switch was used to select the appropriate probes for recording. Thus, there was minimal disturbance to the flow during the recording of the output from the probes. Pearce (1979) has previously used the same method to determine the wave speed at the top and the bottom part of the tube in horizontal annular flow. For some flow conditions, he found the velocity to be higher at the top than at the bottom, but he attributed it to random experimental error.

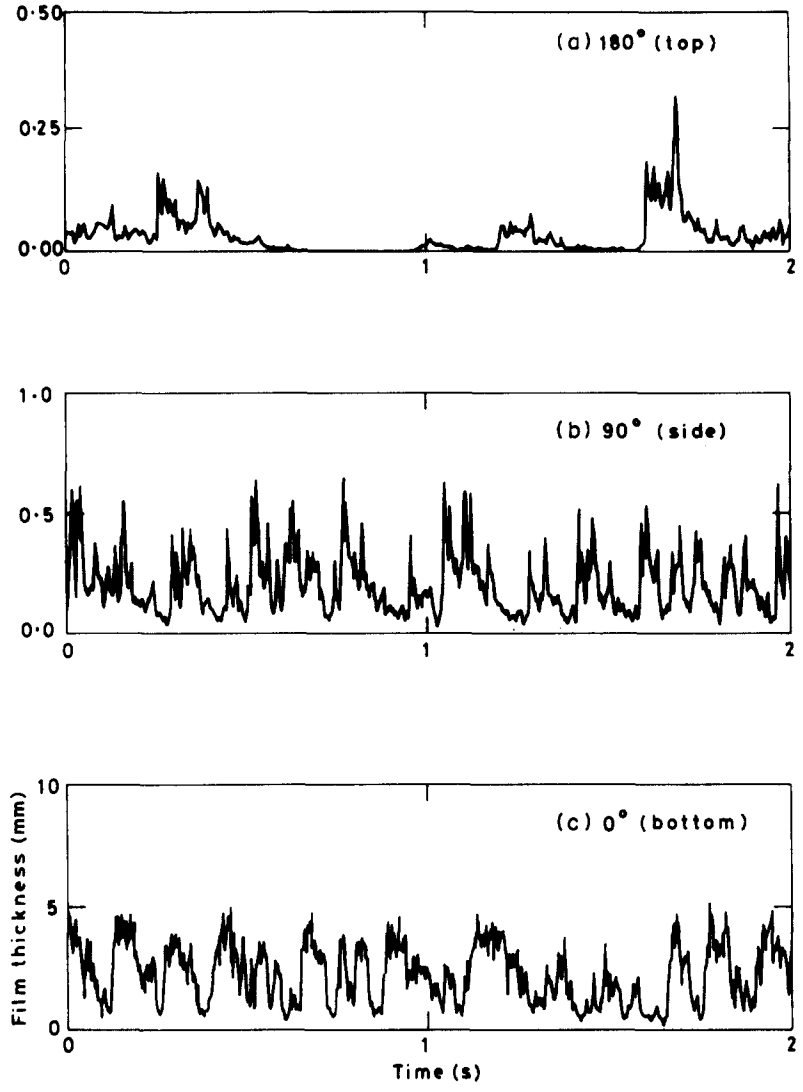

Figure 7. Variation of film thickness with time; water flow rate = 0.118 kg/s and air flow rate = 0.026 kg/s.

Thus the above result, if unphysical, must be due to some systematic error. We offer the following explanation. It has hitherto been tacitly assumed that there is one wave velocity for each set of flow conditions, whereas the ASD functions above show that waves of different frequencies are present. If the waves have different speeds—coalescence of waves has been observed in vertical annular flow—the above method of using cross-correlation in the time domain gives erroneous results; it is best in such circumstances to use cross-correlation in the frequency domain. The wave speed can also be obtained from the slope of the phase part of the CSD function. Figures 14(a, b) show the amplitude (real) and phase (imaginary) parts of the CCF in the frequency domain (CSD). The cross-correlation is between the signals from two probes at the bottom part of the tube, separated by an axial distance of 0.133 m. From the random variation of the phase angle in figure 14(b), it can be concluded that the signals are not coherent for frequencies greater than about 10 Hz. Also, the slope of the phase angle vs frequency curve is different for low (say, <3 Hz) and high (>3 but <10 Hz) frequencies. Using the relation that slope $= 2\pi\tau_0$, where τ_0 is the time delay, it can be shown that the low frequency waves travel with a velocity of 3 m/s, whereas those of higher frequency travel at a lower velocity of 2 m/s for this set of flow conditions. In the CSD at a higher gas flow rate [figures 15(a,b)], where low frequency waves are absent [see the corresponding ASD in figures 10(a–c)] the slope is nearly constant.

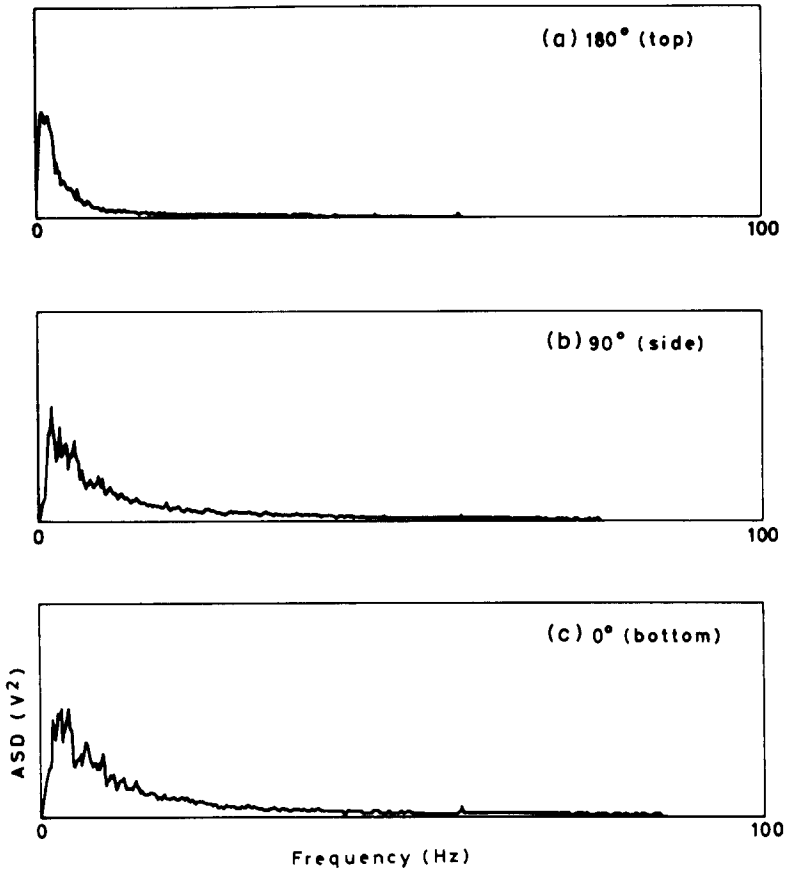

Figure 8. ASDs of the film thickness variation; water flow rate = 0.118 kg/s and air flow rate = 0.026 kg/s.

The above result can be used to explain why waves appear to be moving slower at the bottom part of the tube. As discussed earlier, the dominant wave frequency at the top of the tube is much less than that at the bottom, the difference being more pronounced at low gas flow rates. Thus, the CCF at the top is representative only of low frequency but high speed waves, whereas at the bottom, it is weighted by both low and high frequency waves. As the gas flow rate increases, even the high frequency waves become circumferentially coherent, and the difference in the apparent wave velocity between top and bottom becomes much less, as can be seen from figure 13.

The corrected wave velocities and other wave characteristics are given in table 3.

4. MECHANISMS REVISITED

Certain inferences can be drawn from the above experimental results regarding the presence or otherwise of the mechanisms of film distribution discussed in section 1. It was observed during the experiments that for certain flow conditions (low gas flow rate and high liquid flow rate), the top of the tube was wetted periodically by surges of liquid, and that in between successive surges, the film broke down into small rivulets. Thus, it is unlikely that the surface tension of the liquid can lead to the formation of a continuous film around the circumference in our case.

There were two mechanisms by which the film at the top was replenished. At low gas flow rates, the tube was swept periodically by low frequency surges; in between these surges, the liquid drained down from the top, the tube nearly drying out occasionally at the top. As the flow rate increased, it was observed that a more stable film was formed in the upper part of the tube. Using the spectral analysis results, it can be shown that this is due to some kind of wave spreading mechanism. Figures 16(a–e) show the ASDs of the film at 0° (bottom), 45°, 90°, 135° and 180° for a low gas flow and high liquid flow rate combination. The ASDs at 0° and 45° have peaks at 4–5 Hz (corresponding to the disturbance wave frequency), whereas in the ASD at 90° there appear two peaks—one

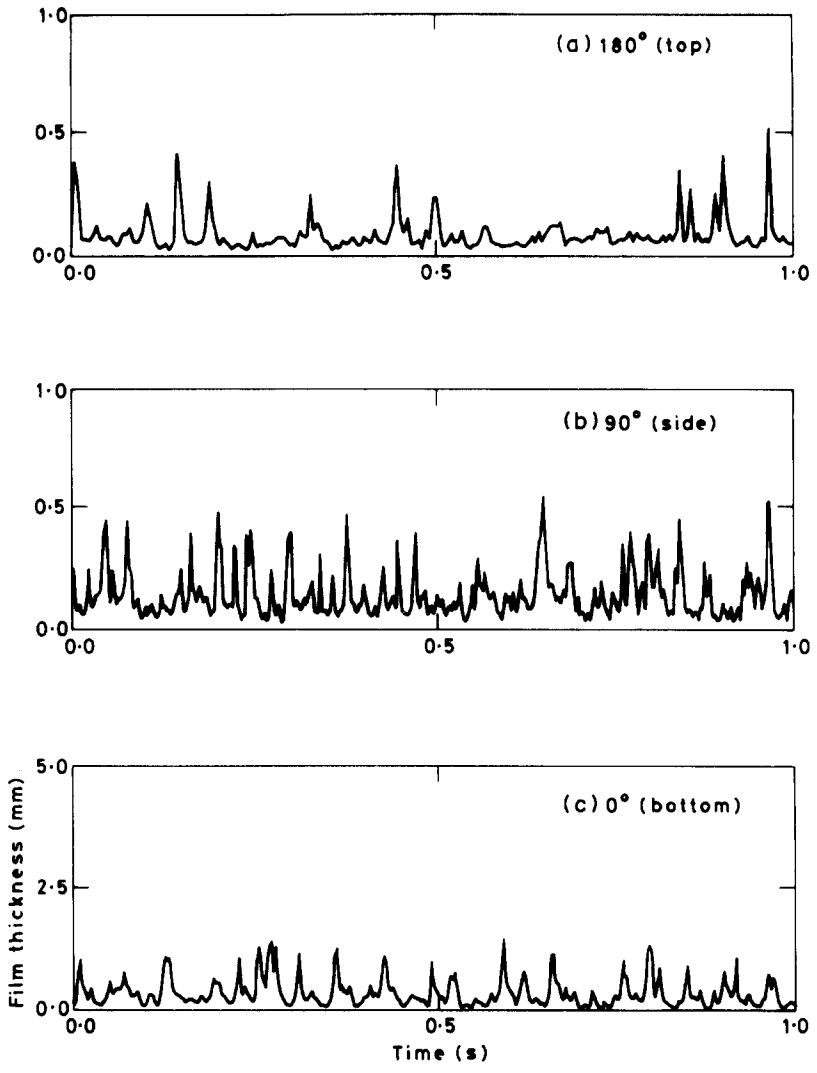

Figure 9. Variation of film thickness with time; water flow rate = 0.064 kg/s and air flow rate = 0.065 kg/s.

corresponding to the disturbance wave frequency of 4–5 Hz, and another at 2–3 Hz. Also, the low frequency peak becomes more predominant as one goes towards the top, with the ASD at 180° showing little trace of the disturbance wave peak. This means that the disturbances waves have very little influence at the top, and hence have "climbed" only up to about 90° for this set of flow conditions. At a higher gas flow rate [figures 17(a–e)], the ASDs up to 135° have a peak corresponding to the disturbance wave frequency showing that they have climbed up to a position of 135° from the bottom. At still higher gas flow rates, the range of dominant frequencies is similar at all circumferential positions [figures 18(a–e)], indicating that the disturbance waves have now spread to the top of the tube. Also, at higher gas flow rates, the disturbance waves become more frequent; the combination of more circumferential spreading and more frequent disturbance waves leads to the formation of a stable film.

It has been suggested that secondary flow in the gas phase can induce a circumferential flow in the film. There are two mechanisms by which a secondary flow in the gas core can be created. Since the mean film thickness is not uniform around the circumference, the gas core effectively flows through a duct of non-circular cross-section. Turbulent flow through such ducts gives rise to secondary flow (Goldstein 1965), as shown in figures 19(a, b) for ducts of square and triangular cross-sections. The flow area for the gas phase in horizontal annular flow is also noncircular, especially when a disturbance wave passes by [figure 19(c)]. Since this cross-section is somewhere between a rectangle and a triangle, this may generate secondary flows—shown schematically in

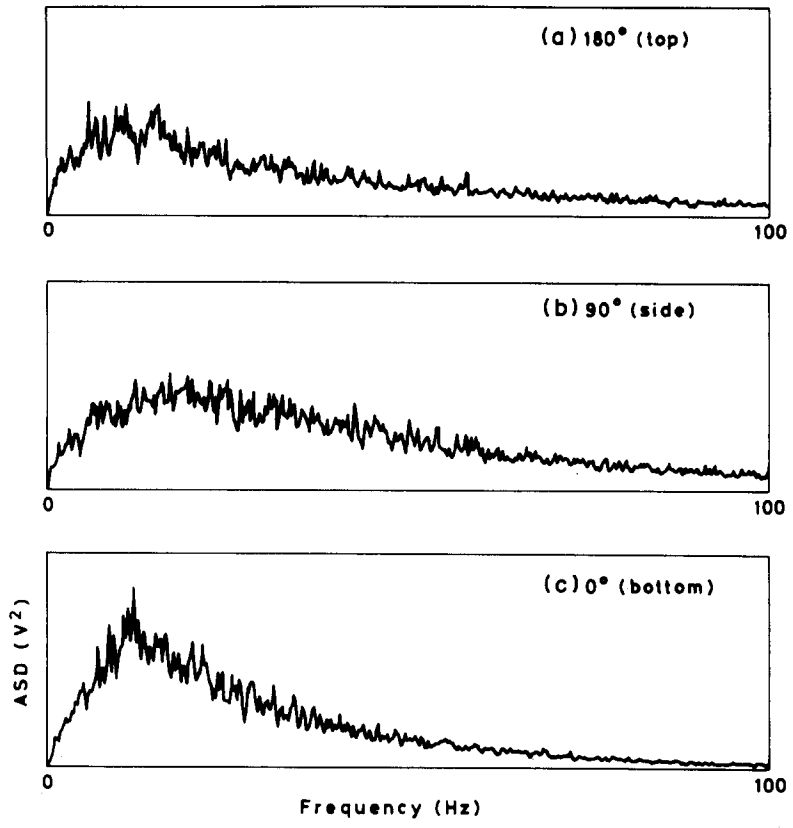

Figure 10. ASDs of the film thickness variation; water flow rate = 0.064 kg/s and air flow rate 0.065 kg/s.

figure 19(c). It is obvious that they cannot transport liquid from the bottom to the top; however, they can contribute to the spreading of the film towards the top, once it reaches the side.

The second mechanism by which secondary flow may be created is the circumferential variation of interfacial shear stress/roughness. Such a variation in single-phase flow creates a two-vortex secondary flow (e.g. Darling & McManus 1968). However, all available experimental evidence points to the absence of strong secondary flow in the gas phase in two-phase horizontal annular flow. The dynamic head (ρv^2) in the gas phase is shown (Krasiakova 1952) to attain a maximum value in the upper half of the tube, whereas, if secondary flow was present, this would occur in the rougher, i.e. lower half (Darling & McManus 1968). Similarly, no effect of secondary flow on the motion of entrained droplets can be observed in the ciné films of horizontal annular flow taken at the Harwell Laboratory. Finally, the measurements of Pearce (1979) show that the ratio of the bottom-to-top wall shear stress is generally between 1 and 1.5. It is doubtful if such a small variation can lead to significant secondary flow; recent calculations carried out at Harwell support this view.

To summarize, our experimental results show that (i) not all disturbance waves are circumferentially coherent, but that (ii) the velocity of circumferentially-coherent waves is essentially constant around the tube, and (iii) the apparent "climbing" of the liquid film along the wall when the gas flow rate is increased (Pletcher & McManus 1965) is due, somehow, to the waves, and not to the secondary flows generated by varying interfacial roughness. It has been suggested by Butterworth (1971) that waves spread along the wall because the wave at the bottom travels faster, and thus is distorted. Our experimental results have not shown the wave velocity at the bottom to be significantly different from that at the top. Also, if the velocities are different around the tube, the waves cannot be coherent axially for long distances. Fukano & Ousaka (1989) also state that the wave crest moves faster at the bottom, although they use mean film thickness to calculate wave velocity in their mathematical model.

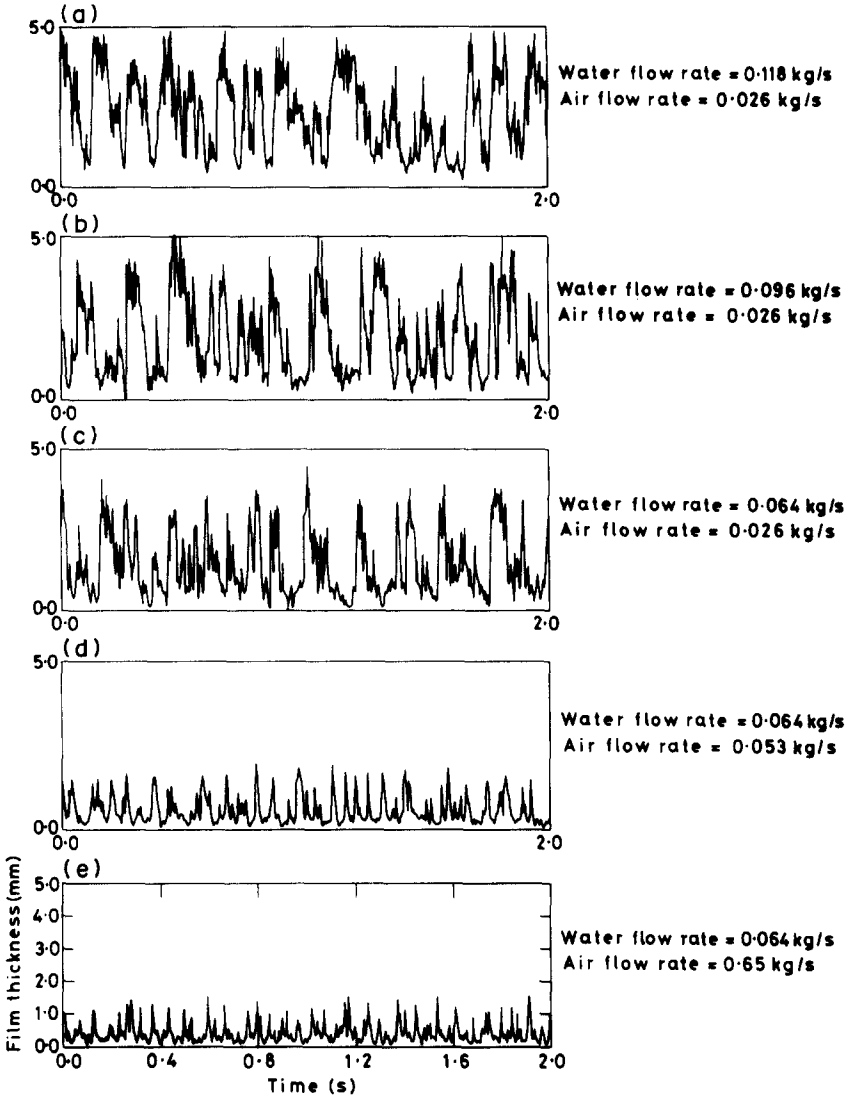

Figure 11. Variation of film thickness at the bottom part of the tube for various flow conditions.

Based on our experimental results, we propose the following mechanism for the spreading of liquid from the bottom to the top. Disturbance waves are created at the bottom part of the tube. At this point, they are not circumferentially coherent, and the axial velcoity changes around the tube. Because of this, they get distorted as they travel downstream [through the mechanism of Butterworth (1971)], and become circumferentially coherent [figure 20(a)]. In the process, they also become "inclined", with the bottom part of the wave being further downstream than the top part. From this point on, the wave travels with constant velocity, and become axially coherent over long distances. Thus, the wave acts as a solid entity sweeping through the liquid film. Since the wave

Table 2. Mean film thickness as a function of circumferential position and flow conditions

S. No.	Water flow rate ($kg\,s^{-1}$)	Air flow rate ($kg\,s^{-1}$)	Mean film thickness (mm) at 0° (bottom)	45°	90°	135°	180°
1	0.118	0.026	1.53	1.06	0.35	0.20	0.11
2	0.096	0.026	1.28	0.87	0.31	0.19	0.11
3	0.064	0.026	0.87	0.68	0.25	0.16	0.04
4	0.064	0.053	0.36	0.33	0.24	0.18	0.14
5	0.064	0.065	0.29	0.26	0.22	0.18	0.14

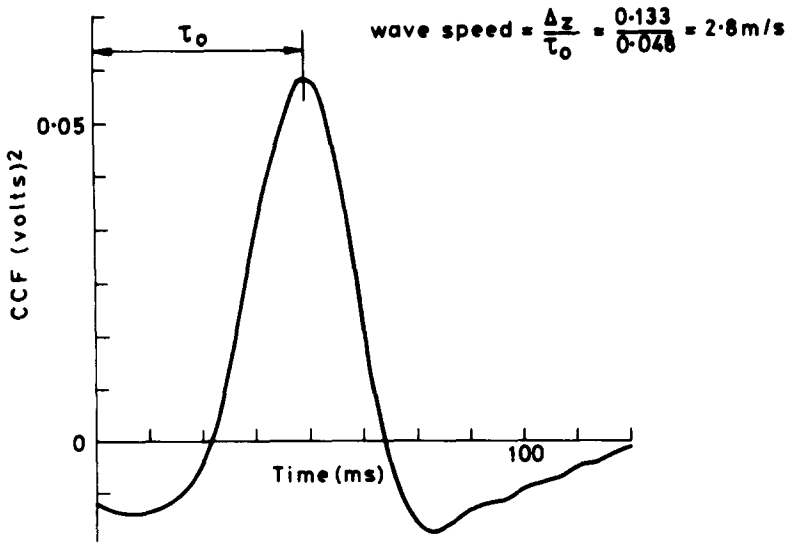

Figure 12. CCF of voltage signals from two probes at 0° (bottom) separated by an axial distance of 0.133 m; water flow rate = 0.064 kg/s and air flow rate = 0.053 kg/s. The peak occurs after a delay of 48 ms.

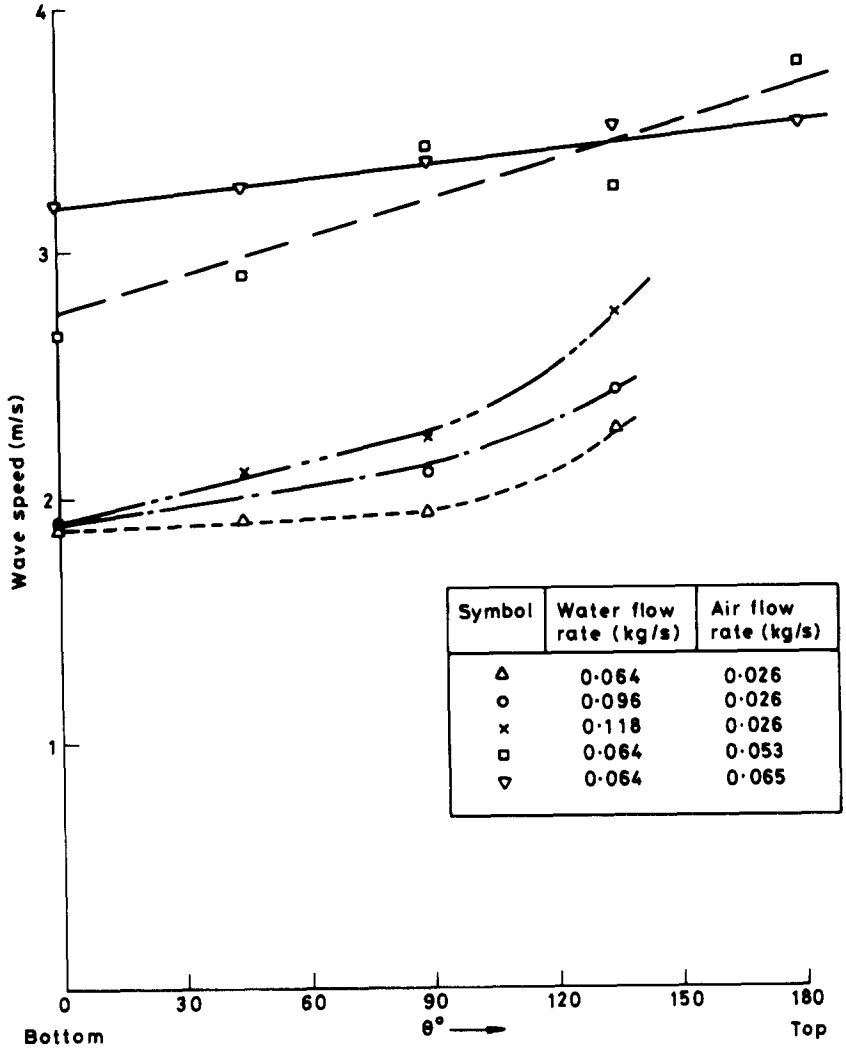

Figure 13. Wave speeds obtained from CCFs.

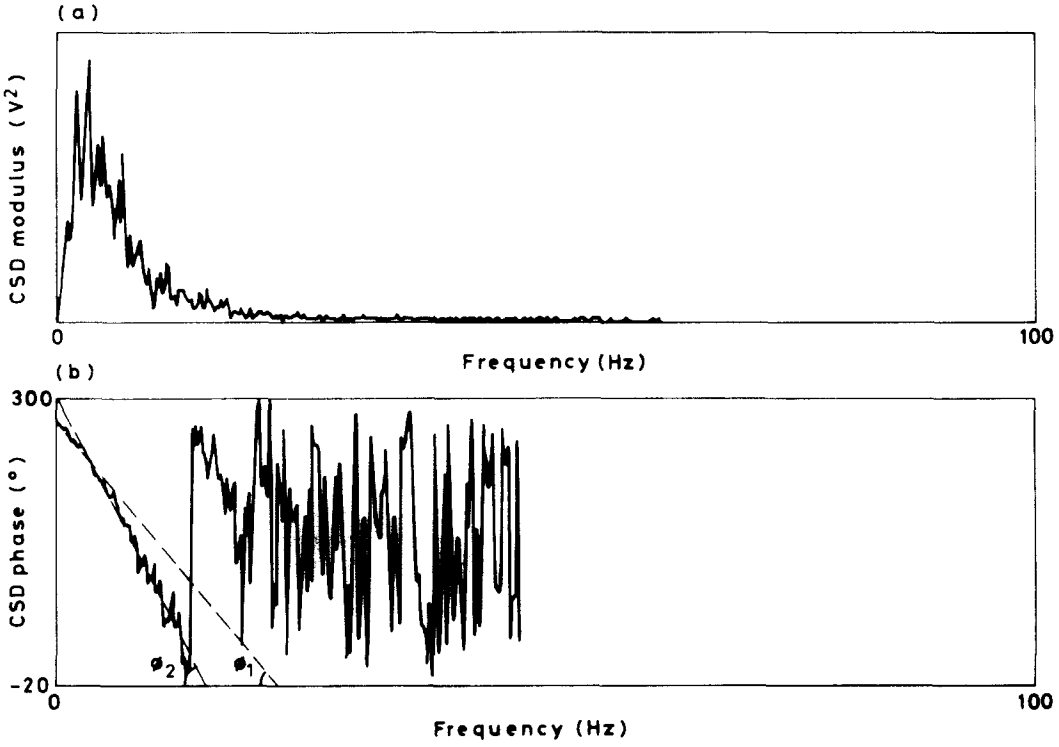

Figure 14. CSD: (a) real part; (b) imaginary part. Voltage signals are from two probes at the bottom part of the tube separated by an axial distance of 0.133 m; water flow rate = 0.118 kg/s and air flow rate = 0.026 kg/s. Note that the slope is not the same at all frequencies.

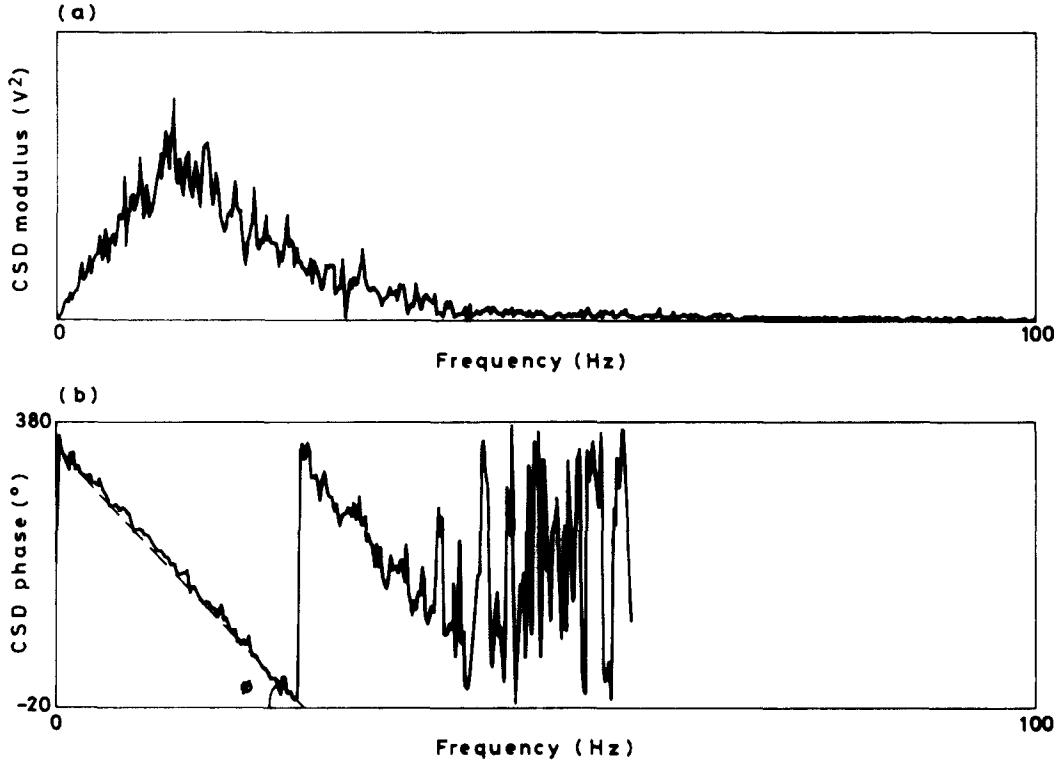

Figure 15. Same as in figures 14(a,b) but at a water flow rate of 0.064 kg/s and an air flow rate of 0.065 kg/s. Note that the slope in (b) is constant.

Table 3. Disturbance wave characteristics

S. No.	Water flow rate ($kg\,s^{-1}$)	Air flow rate ($kg\,s^{-1}$)	Disturbance wave[a]				Mean film thickness (mm)	Wave height
			Frequency (Hz)	Velocity ($m\,s^{-1}$)	Spacing[b] (m)	Height (mm)		Mean film thickness
1	0.118	0.026	2–4	1.9	0.53	>4.0	1.53	>2.6
2	0.096	0.026	2–5	1.9	0.48	>2.0	1.28	>3.1
3	0.064	0.026	4–6	1.8	0.36	3.75	0.87	4.3
4	0.064	0.053	6–12	2.9	0.32	1.6	0.36	4.4
5	0.064	0.065	7–14	3.2	0.30	1.25	0.29	4.3

[a]At the bottom part of the tube ($\theta = 0°$).
[b]spacing $= \frac{\text{frequency}}{\text{velocity}}$.

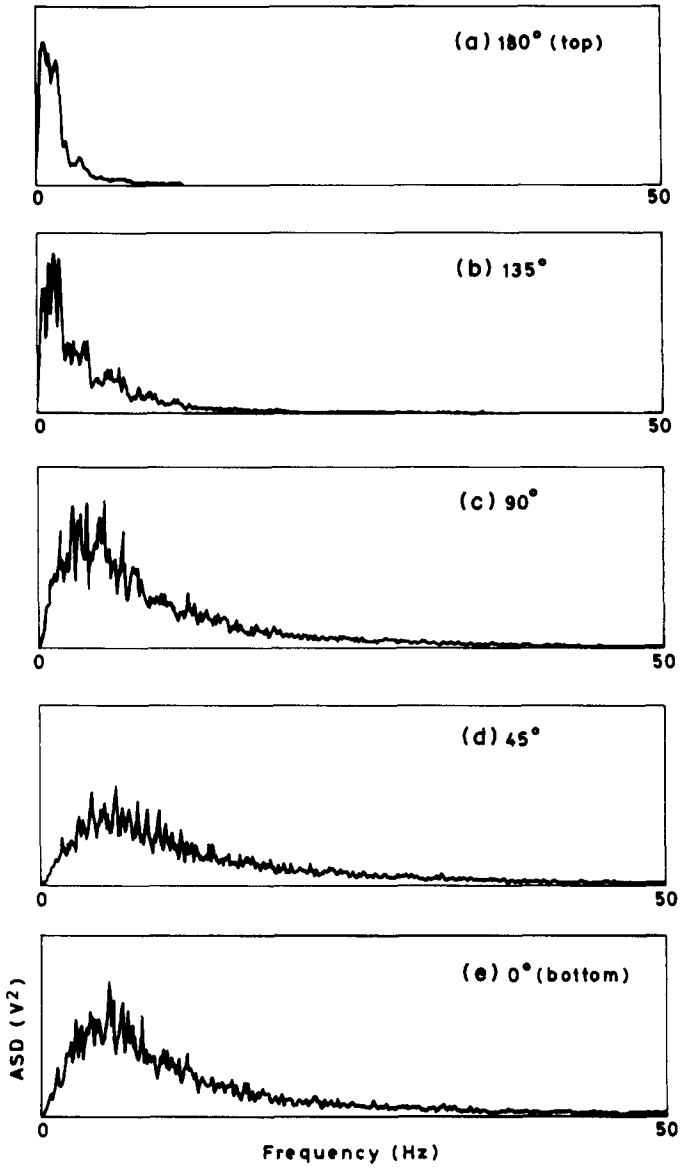

Figure 16. ASDs at different circumferential positions; water flow rate = 0.096 kg/s and air flow rate = 0.026 kg/s.

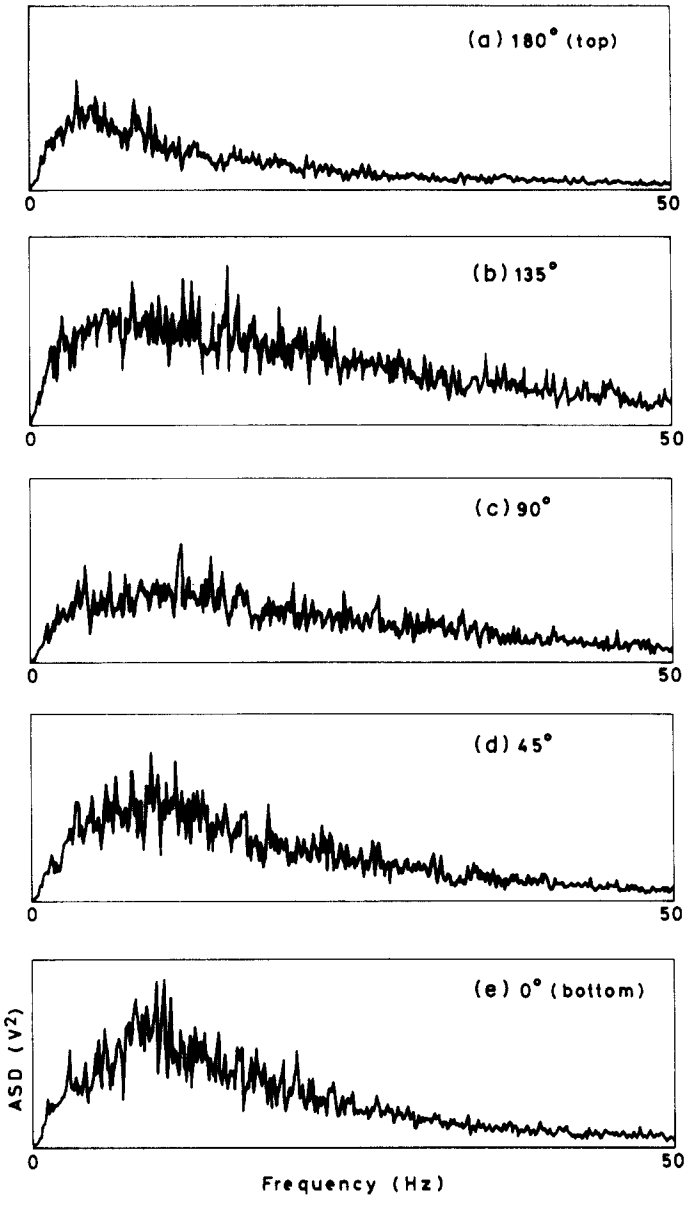

Figure 17. Same as in figures 16(a–e) but at an air flow rate of 0.053 kg/s.

velocity is higher than that of the mean film, the liquid is deflected from the tip of the wave towards the sides [figure 20(c)], thus climbing from the bottom towards the top. Thus, the liquid climbs downstream of the wave, and drains upstream. It should be noted that this scenario is consistent with all the experimental results obtained so far.

The key to the above model is the inclination of disturbance waves. We have established this experimentally in the following way. Film thickness was measured simultaneously at the bottom and the side of the tube. The measurements were done using parallel plate conductance probes [of the type used by Webb (1970)] in a Plexiglas tube of 38 mm (1.5″) i.d. The resulting film thickness signals were cross-correlated using the Solartron 1200 spectrum analyser. If the CCF peaked at zero time lag, it would mean that disturbance waves arrived at both the bottom and the side at the same time [figure 21(a)]; if not, the wave would not arrive at both points simultaneously, and the wave front would be ahead either at the bottom [figure 21(b)] or at the side [figure 21(c)]. The CCF in our measurements was of the type shown in figure 21(b). The delay time was of the order of a few milliseconds (table 4), and was much less than the least count of the time scale. (During several samplings of a 4-min long signal, the delay time varied only by one or two least counts

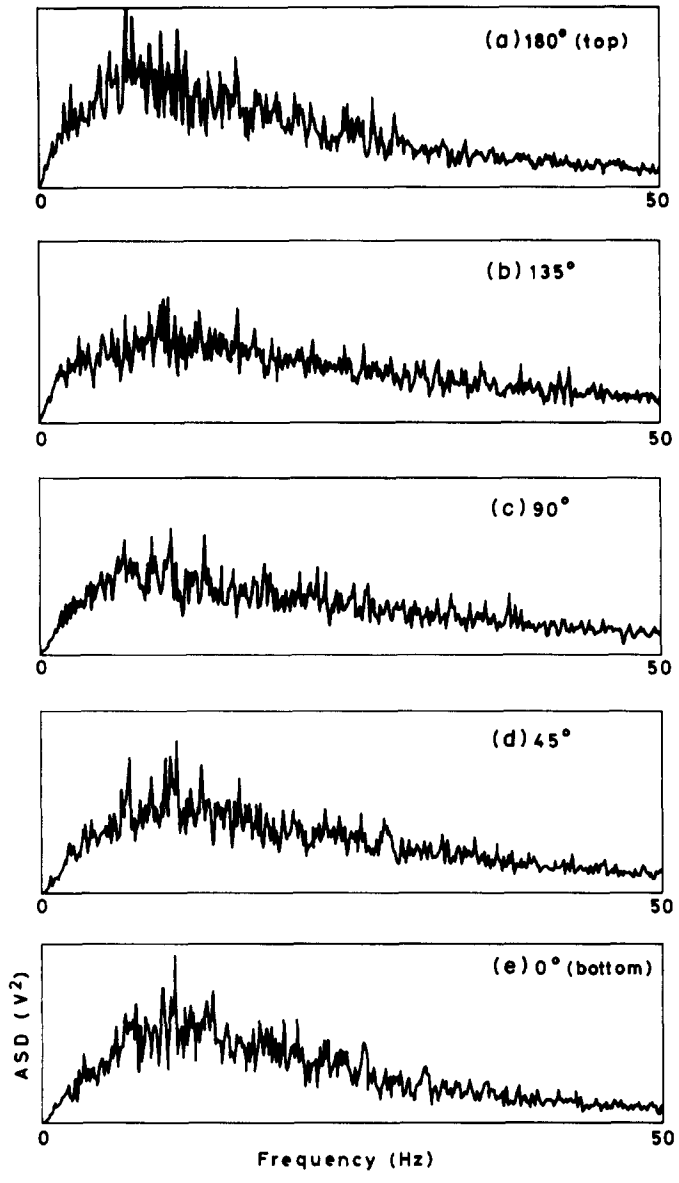

Figure 18. Same as in figures 16(a–e) but at an air flow rate of 0.065 kg/s.

Table 4. Delay time (t_d) in the cross-correlation of the film thickness at the bottom and at the side in air–water horizontal annular flow

S. No.	Air flow rate ($kg\,s^{-1}$)	Water flow rate ($kg\,s^{-1}$)	Superficial velocity		Delay time ± least count (ms)
			Air ($m\,s^{-1}$)	Water ($m\,s^{-1}$)	
1	0.038	0.112	19	0.10	-4.5 ± 0.3
2	0.057	0.112	28	0.10	-3.6 ± 0.3
3	0.077	0.112	38	0.10	-1.1 ± 0.1
4	0.094	0.112	46	0.10	-0.7 ± 0.1
5	0.063	0.059	31	0.05	-2.7 ± 0.3
6	0.077	0.059	38	0.05	-1.6 ± 0.1
7	0.027	0.139	13	0.12	-4.4 ± 0.3

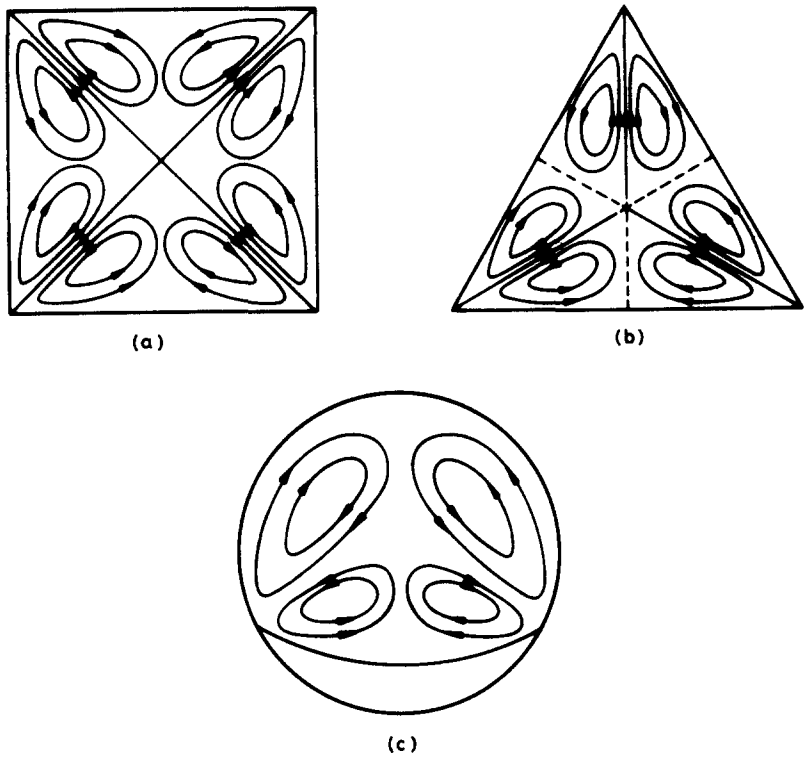

Figure 19. (a,b) Turbulence-driven secondary flow in non-circular ducts. (c) Possible secondary flow induced by the same mechanism in the gas phase in horizontal annular flow when a disturbance wave passes by.

of the time scale.) These results can only mean that the disturbance waves are "inclined", as shown in figures 20(a–c). Assuming a typical wave velocity of 2–3 m/s, the wave should be ahead at the bottom by about 5–10 mm. Note that the decrease in the delay time with increasing air flow rate (table 4) is consistent with the scenario presented above.

5. CONCLUSIONS

In the present study, the time-dependent behaviour of the liquid film in horizontal annular flow is investigated. The following conclusions can be drawn from this study.

At high liquid flow rates and low gas flow rates, the liquid film is affected by "disturbance" waves of frequencies of the order of 5 Hz. As the gas flow rate is increased, the disturbance wave frequency increases; also, the range of the frequency of waves broadens.

For a given set of flow conditions, the dominant wave frequency in the upper part of the tube is less than that in the lower part of the tube; this difference decreases as the gas flow rate is increased. Thus, for low gas flow rates, the disturbances waves at the bottom of the tube have little influence on the liquid film at the top. However, as the gas flow rate increases, they spread towards the top along the tube wall. The combination of more circumferential spreading and more frequent waves leads to the formation of a stable layer of liquid film in the upper part of the tube.

The disturbance waves at the bottom of the tube have a speed of about 2–4 m/s. All circumferentially-coherent waves travel with the same speed. Circumferential cross-correlation shows that waves are inclined with the wave front being ahead at the bottom other than at the side. A new mechanism is proposed by which this inclination transfers liquid from the bottom to the top.

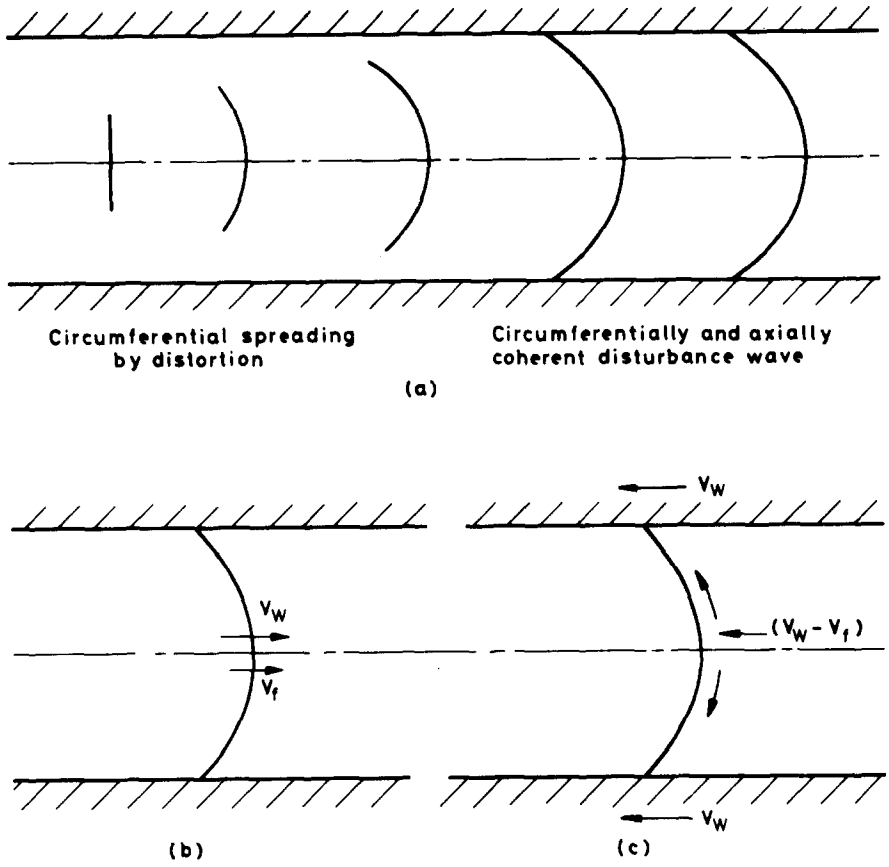

Figure 20. (a) Circumferential spreading of a disturbance wave after inception. (b) A disturbance wave in fully developed flow; V_w = wave velocity and V_f = film velocity. (c) Secondary motion in the liquid due to a disturbance wave moving faster than the film.

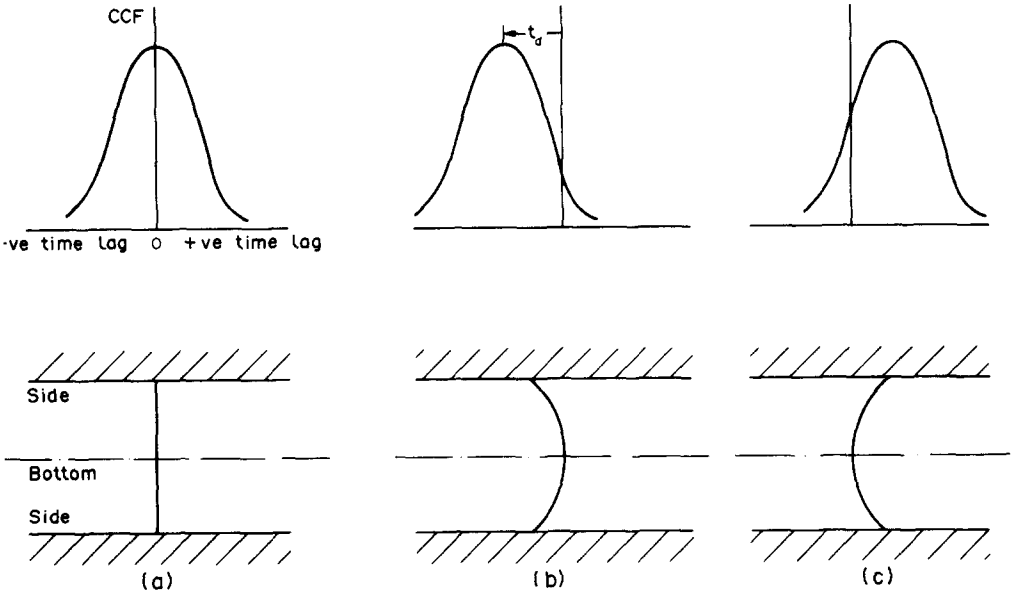

Figure 21. The relation between shape of the wave front and the CCF between the film thickness at the bottom and at the side: (a) no delay; (b) negative delay; (c) positive delay.

Acknowledgements—The authors wish to thank Drs B. J. Azzopardi and H. G. D. Goyder and their co-workers for useful discussions.

REFERENCES

ANDERSON, R. J. 1968 Interchange in horizontal annular two-phase flow. Ph.D. Thesis, Univ. of Delaware, Newark.

BENDAT, J. S. & PEARSOL, A. G. 1986 *Random Data: Analysis and Measurement Procedures*, 2nd edn (revised and enlarged). Wiley, New York.

BUTTERWORTH, D. 1971 Air–water annular flow in a horizontal tube. UKAEA Report No. AERE-R6687.

BUTTERWORTH, D. & PULLING, D. J. 1972 A visual study of mechanisms in horizontal annular air–water flow. UKAEA Report No. AERE-M2556.

CONEY, M. W. E. 1971 The variation of liquid film thickness in horizontal two-phase flow. CERL Report No. CERL/RD/L/N 273/71.

DARLING, R. S. & MCMANUS, H. N. 1968 Flow patterns in circular ducts with circumferential variation of roughness: a two-phase flow analogue. In *Proc. 11th Mid-Western Mechanics Conf.*, Paper 9, pp. 153–163.

FUKANO, T. & OUSAKA, A. 1989 Prediction of the circumferential distribution of film thickness in horizontal and near-horizontal gas–liquid annular flows. *Int. J. Multiphase Flow* **15,** 403–419.

FUKANO, T., OUSAKA, A., MORIMOTO, T. & SEKOGUCHI, K. 1983 Air–water annular two-phase flow in a horizontal tube (Part II: circumferential variation of film thickness parameters). *Bull. JSME* **26**(218), 1387–1395.

GOLDSTEIN, S. 1965 *Modern Developments in Fluid Dynamics*, Vol. II (Edited by GOLDSTEIN, S.). Dover, New York.

HEWITT, G. F., JAYANTI, S. & HOPE, C. B. 1989 Structure of thin liquid films in gas–liquid horizontal annular flow. UKAEA Report No. AERE-R13643.

KRASIAKOVA, L. I. 1952 Some characteristic flows of a two-phase mixture in a horizontal pipe. *Zh. Tech. Fiz.* **22,** 656.

LAURINAT, J. E., HANRATTY, T. J. & JEPSON, W. P. 1985 Film thickness distribution for gas–liquid annular flow in a horizontal pipe. *PhysicoChem. Hydrodynam.* **6,** 179–195.

LIN, T. F., JONES, O. C., LAHEY, R. G., BLOCK, R. C. & MURASE, M. 1985 Film thickness measurements and modelling in horizontal annular flows *PhysicoChem. Hydrodynam.* **6,** 197–206.

MARTIN, C. J. & AZZOPARDI, B. J. 1985 Waves in vertical annular flow. *PhysicoChem. Hydrodynam.* **6,** 257–265.

MCMANUS, H. N. 1959 An experimental investigation of liquid distribution and surface character in horizontal annular two-phase flow. Interim Report Nos 1 & 2, Sibley School of Mech. Engng, Cornell Univ., Ithaca, N.Y.

OLIEMANS, R. V. A. & OOMS, G. 1986 Core annular flow of oil and water through a pipe line. In *Multiphase Science Technology*, Vol. 2, Chap. 6 (Edited by HEWITT, G. F., DELHAYE, J. M. & ZUBER, N.). Hemisphere, New York.

PEARCE, D. L. 1979 Film waves in horizontal annular flow: space–time correlator experiments. CEGB Report No. CERL/RD/L/N 111/79.

PEARCE, D. L. & FISHER, S. A. 1976 Theoretical and experimental investigation of dryout in horizontal annular flows: preliminary report. CEGB Report No. CERL/RD/L/N 193/75.

PLETCHER, R. H. & MCMANUS, H. N. 1965 The fluid dynamics of three-dimensional liquid films with free surface shear: a finite difference approach. In *Proc. 9th Mid-Western Mechanics Conf.*, Wisc.

RUSSELL, T. W. F. & LAMB, D. E. 1965 Flow mechanism of two-phase annular flow. *Can. J. chem. Engng* **43,** 237–245.

WEBB, D. R. 1970 Studies of the characteristics of downward annular two-phase flow: parts 1–5. UKAEA Report No. AERE R6426.

WILKES, N. S., CONKIE, W. & JAMES, P. W. 1980 A model for the droplet deposition in horizontal annular two-phase flow. UKAEA Report No. AERE-R9691.